Complexity Project

CID: 01854896

20th February 2023

Abstract: The Oslo model was implemented to test for characteristics that are commonly displayed in models with self organised criticality, namely the possibility for power-law scaling and data collapse. System sizes of $L \in \{4, 8, 16, 32, 64, 128, 256, 512, 1024\}$ were analysed, and data collapses were produced for the height at the first lattice site h, the probability of height configurations with height h, and the probability of avalanches of a certain size s. Additionally, several exponents in power-law relations were measured, where $\tilde{h} \sim t^{0.503}$ in the transient, $\sigma_h \sim L^{0.242}$. The moment scaling analysis was used to yield $D = 2.2524 \pm 0.0014, \tau_s = 1.5561 \pm 0.0007$. By using $L = 1024$ for measurements, this attempted to mitigate errors arising from small L effects, which caused deviations in the power-law relation. However, there still remains a small bias that is not quantified by our quoted uncertainty.

Word count: 2435 words in report (excluding front page, figure captions, table captions, and bibliography).

1 Introduction

The Oslo Model was implemented and analysed for different number of lattice sites, also referred to as the system size and denoted by L. Unless explicitly stated, the analysis was performed for $L \in \{4, 8, 16, 32, 64, 128, 256, 512, 1024\}$. The implementation of the algorithm was incorrect for $L = 1$, because the first and last site overlap but have conflicting relaxation methods. This was not an issue for the remainder of the project as all instances of the Oslo Model, referred to as systems, have $L \neq 1$.

1.1 Task 1a

1.1.1 Mean height of the pile $\langle h(t; L)\rangle_t$ in the steady state

The height of the pile, $h(t; L)$, is defined to be the height at site $i = 1$, the leftmost site in a stable configuration. Making a (currently unjustified) assumption that each h over time is independent in the steady state, the standard error can be calculated from $\sigma_{\langle h\rangle} = \sigma/\sqrt{T}$. $L = 16, 32$ systems were brought to the steady state by running for $t = 400, 1500$ respectively, where each timestep t increments by one per grain dropped. Then, each system was run for a further $T = 3\,000\,000$, where T is hereon the number of timesteps ran after $t > t_0$, and t_0 is some time in the steady state.

$$\langle h(t; 16)\rangle_t = 26.5308 \pm 0.0006$$
$$\langle h(t; 32)\rangle_t = 53.8896 \pm 0.0008$$

This agrees with the values given in the project script up to the quoted precision.

1.1.2 Recurrent configurations, $N_{\mathcal{R}}$

The number of recurrent configurations is given in Equation (1), where each recurrent configuration is an ordered list of z_i that remains accessible for $t > t_c$.

$$N_{\mathcal{R}} = \frac{1}{\sqrt{5}}\left(\phi(1+\phi)^L + \frac{1}{\phi(1+\phi)^L}\right). \tag{1}$$

Only systems of small $L \in \{2, 3, 4, 5\}$ were tested, as the t required to explore the set of all recurrent configurations, $\mathcal{R}$, rapidly rises with increasing L. We set $T = 10\,000\,000$ such that it was highly likely to find all recurrent configurations for large L with any given seed, whilst also giving sufficient timesteps for the simulated $N_{\mathcal{R}}$ to exceed the theoretical $N_{\mathcal{R}}$ if the implementation was incorrect. The results are given in Table 1. The simulated $N_{\mathcal{R}}$ indeed matched the theoretical $N_{\mathcal{R}}$.

L	Simulated $N_{\mathcal{R}}$	Theoretical $N_{\mathcal{R}}$
2	5	5
3	13	13
4	34	34
5	89	89

Table 1: A comparison for the number of recurrent configurations, $N_{\mathcal{R}}$, as found by simulation and from Equation (1) for different L. They matched exactly for $T = 10\,000\,000$, indicating the model performed as expected.

1.1.3 BTW recurrent configuration test

Setting $p = 0$ for the threshold slope z_i^{th} turns the Oslo model into the BTW model. This model only has one recurrent configuration, namely the 'staircase' configuration. Representing this visually in a matrix of heights, this should appear as a lower triangular matrix

$$\begin{bmatrix} 1 & 0 & 0 & \dots & 0 \\ 1 & 1 & 0 & \dots & 0 \\ 1 & 1 & 1 & \dots & 0 \\ \vdots & \vdots & \vdots & \ddots & \vdots \\ 1 & 1 & 1 & \dots & 1 \end{bmatrix}_{L \times L}$$

where 1 represents a filled block at a coordinate in space, and 0 otherwise. The length of the filled 1's in column i is the height at site i. To test this, $L = 8$ was ran for $T = 100\,000$ in the steady state. The model passed the test where at every t, the stable configuration was checked to be exactly this matrix.

2 The height of the pile $h(t; L)$

2.1 Task 2a

$h(t; L)$ was plotted against the time t, shown in Figures 1, 2.

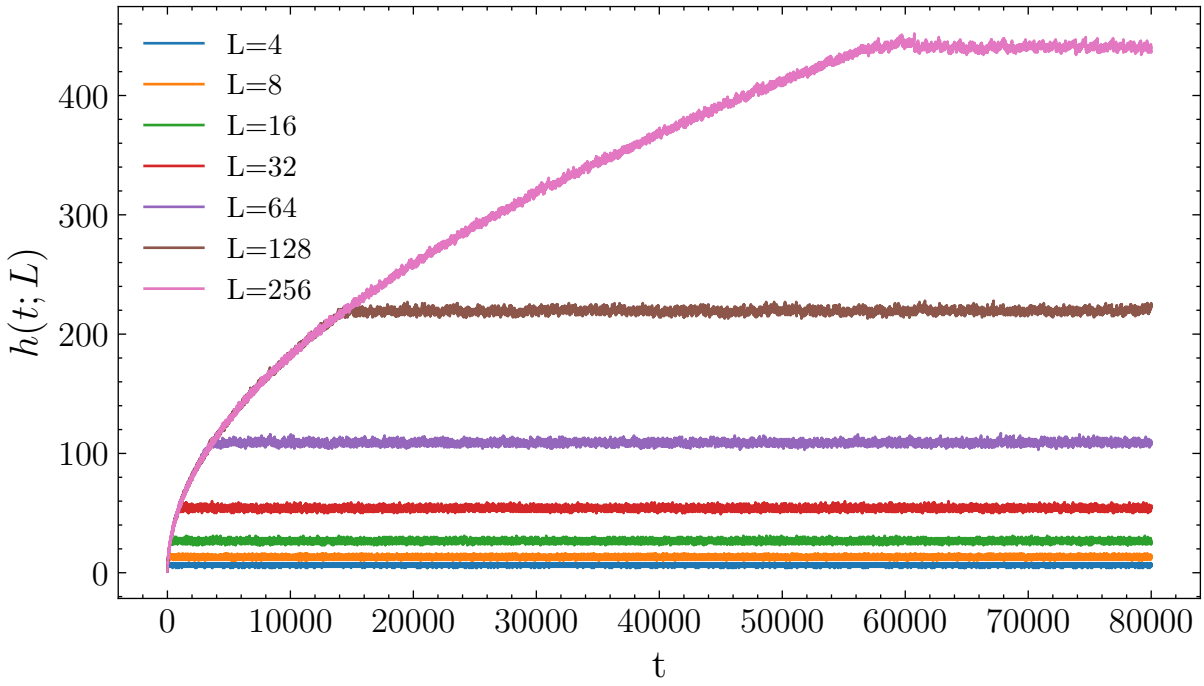

Figure 1: Plot of $h(t; L)$ against t for system sizes up to $L = 256$. Visually, the time taken to reach the steady state, indicated by the turning point where h flattens out, grows exponentially with L.

From Figure 1, h roughly increases sublinearly, until it reaches a point and then oscillates around a flat line with mean $\langle h \rangle_t$. Before this point, the system evolves through its recurrent configurations, because each configuration's associated h is small and, for some t later, h has risen enough such that the previous transient configuration can never be revisited again. By contrast, the oscillations around a flat line indicates the characteristic of having reached the

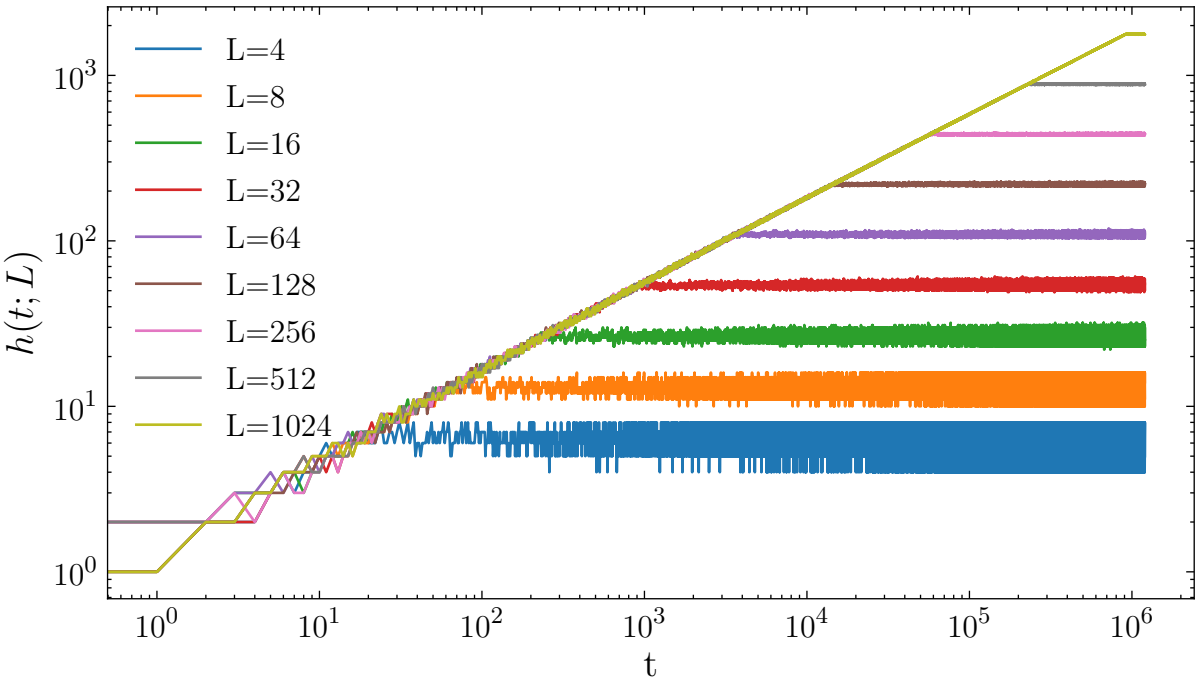

Figure 2: Log-log plot of $h(t;L)$ against t for system sizes up to $L = 1024$. The log-log plot reveals a straight line in the transient region $\forall L$, implying a power-law relation between h and t. Although visually the oscillations in the steady state appear greater for small L, this is an artefact from the log-log scale which emphasises low h values.

recurrent configurations: that is $\langle \text{influx} \rangle = \langle \text{outflux} \rangle$, since the grain added at site $i = 1$ must be counteracted by a grain leaving at $i = L$ on average for h to stabilise.

2.2 Task 2b

The crossover time $t_c(L)$ is defined as the number of grains required before the next grain induces a grain to leave the system. $\langle t_c(L) \rangle$ was computed by averaging $M = 10$ realisations of the same L. Each t_c should be independent since the model was completely reinitialised, and thus $\sigma_{\langle t_c \rangle} = \sigma_{t_c}/\sqrt{M}$, where σ_{t_c} is the numerically estimated standard deviation for a single t_c measurement.

Assuming $\langle t_c(L) \rangle = bL^\beta$ such that it followed a power law, the data was linearised by taking logarithms on both axes. Because $\langle t_c(L) \rangle$ has an uncertainty, this was propagated through the logarithm by using the first order Taylor expansion as in Equation (2).

$$\sigma_{\log \langle t_c \rangle} = \left| \frac{\mathrm{d} \left(\log \langle t_c \rangle \right)}{\mathrm{d}x} \right| \sigma_{\langle t_c \rangle} = \frac{\sigma_{\langle t_c \rangle}}{\langle t_c \rangle}. \tag{2}$$

A linear least squares fit was performed for $L \geq 128$ to approximate $L \gg 1$, weighted by $1/\sigma_{\log \langle t_c \rangle}$, and the error in the exponent β was computed by taking the square root of the relevant element in the diagonal of the covariance matrix. This same procedure was used for the remainder of the project to extract any exponent and its associated error in a power-law relation. From the fit, this gave the value of

$$\beta = 2.007 \pm 0.001$$
$$b = 0.819 \pm 0.005.$$

To check that fitting over $L \geq 128$ was valid, $\langle t_c \rangle / L^2$ was plotted against L on Figure 3, after conjecturing that the true value is $\beta = 2$. Should the power law be the exact form, all

points should lie on a horizontal line indicating $\langle t_c \rangle / L^2 = b$. The last four data points lie almost horizontally, implying $L \geq 128$ was sensible and that most small L effects were avoided. However, the last four data points still exhibit a slight negative curvature, almost flattening to becoming constant. Hence, this fit has a systematic error of being an overestimate of β, and this error was not reflected in the quoted uncertainty.

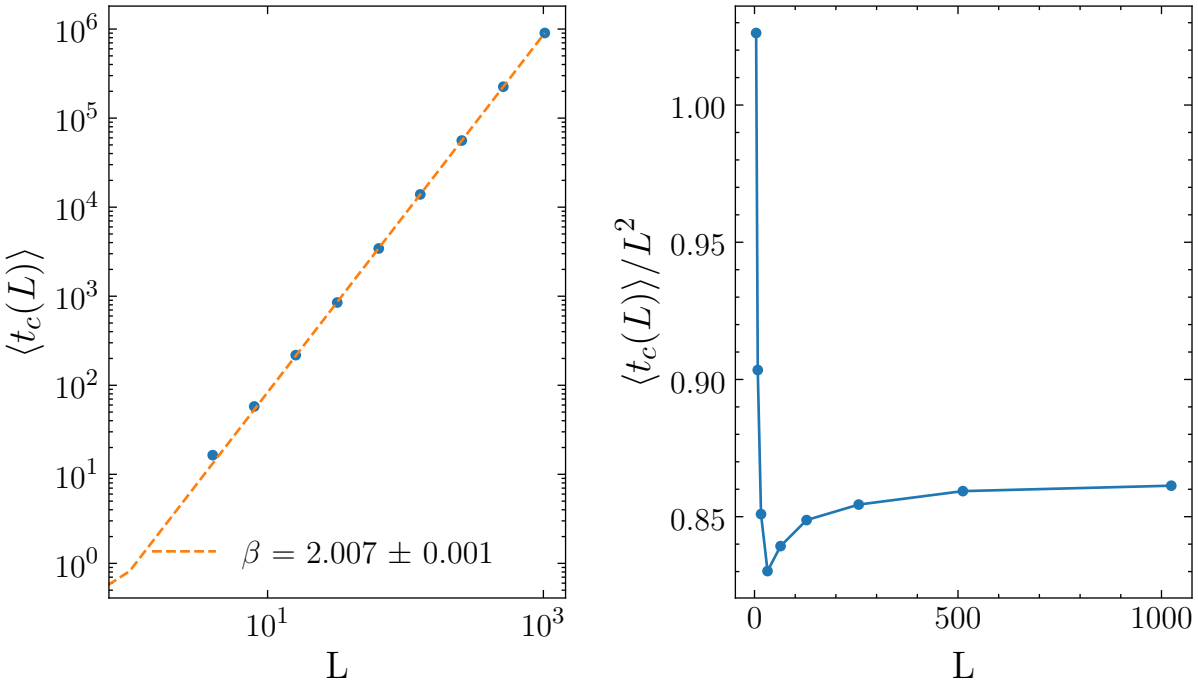

Figure 3: (Left) A weighted linear fit on the log-log plot of $\langle t_c(L) \rangle$ against L, leading to the exponent $\beta = 2.007 \pm 0.001$. Assuming the true value is $\beta = 2$, (Right) illustrates the small L effects by diving the y-axis by L^2, as data points for small L are not flat as expected. Error bars represented by 1 standard deviation were too small to be shown.

2.3 Task 2c

2.3.1 Scaling of h with L

Consider

$$\begin{aligned} \langle h(t;L) \rangle_t &= \frac{1}{T} \sum_{t=t_0+1}^{t_0+T} h(t;L), \\ &= \frac{1}{T} \sum_{t=t_0+1}^{t_0+T} \sum_{i=1}^{L} z_i(t). \end{aligned}$$

Recall that the drive algorithm is different for 2 sites only, namely $i \in \{1, L\}$. For $L \gg 1$, these boundary effects have decreased significance, as more sites tend to an identical driving algorithm. Hence each z_i tend to a mean $\langle z \rangle_i$, where the subscript is a reminder that this is a spatial average,

$$\begin{aligned} \langle h(t;L) \rangle_t &= \frac{1}{T} \sum_{t=t_0+1}^{t_0+T} L \langle z \rangle_i, \qquad \text{for } L \gg 1 \\ &\propto L \langle z \rangle_i, \\ &\sim L, \end{aligned}$$

where $\sim$ denotes 'scales as'.

2.3.2 Scaling of $\langle t_c(L) \rangle$ with L

A geometric argument is made similar to the BTW model in lectures. Firstly, consider the lower bound for t_c for some L, which can be viewed as the least number of grains in a recurrent configuration. This is when $z_i^{th} = 1, \forall i \in L$,

$$\begin{aligned}
\min t_c(L) &= L + (L-1) + (L-2) + \cdots + 1 \\
&= \sum_{i=1}^{L} [L - (i-1)] \\
&= \frac{L(L+1)}{2} \\
&\approx \frac{L^2}{2} \quad \text{for } L \gg 1
\end{aligned}$$

Likewise, the upper bound for t_c is when $z_i^{th} = 2, \forall i \in L$.

$$\begin{aligned}
\max t_c(L) &= (2L) + (2L-2) + (2L-4) + \cdots + 2 \\
&= \sum_{i=1}^{L} [2L - 2\,(i-1)] \\
&= L(L+1) \\
&\approx L^2 \quad \text{for } L \gg 1
\end{aligned}$$

Hence $\langle t_c(L) \rangle$ is constrained between the two,

$$\begin{aligned}
\langle t_c(L) \rangle &\propto bL^2, \quad b \in [0.5, 1] \\
&\sim L^2,
\end{aligned}$$

and indeed the numerically simulated value for b was within $[0.5, 1]$ as found in Task 2b.

2.4 Task 2d

Define $\tilde{h}(t; L) = \left(\sum_{j=1}^{M} h^j(t; L) \right) / M$. This smoothed out the data, reducing the magnitude of oscillations, or visually the 'fuzziness' as depicted in Figure 1 in both the transient and steady state. M was chosen to be different for each L such that visually, each graph appeared smooth; this meant M was greater for small L because their σ_h / L, the fluctuations relative to the system size, was greater. Since $\tilde{h}(t; L) \sim L$ and $\langle t_c(L) \rangle \sim L^2$, dividing by these scalings in L produced data overlaid on top of each other, as they were independent in L. Consequently, the scaling ansatz was hypothesised to be:

$$\tilde{h}(t; L) \propto \langle h \rangle \mathcal{F}\left(\frac{t}{\langle t_c \rangle} \right) = L \mathcal{F}\left(\frac{t}{L^2} \right), \tag{3}$$

where $\mathcal{F}$ is the scaling function. In fact, dividing Equation (3) by L yields

$$\frac{\tilde{h}(t; L)}{L} = \mathcal{F}\left(\frac{t}{L^2} \right), \tag{4}$$

where $x = t/L^2$ and is plotted in Figure 4. From this, the behaviour of $\mathcal{F}$ was inferred as:

$$\mathcal{F}(x) \propto \begin{cases} x^{\alpha} & x \ll 1 \\ \text{const} = a_0 & x \gg 1 \end{cases} \tag{5}$$

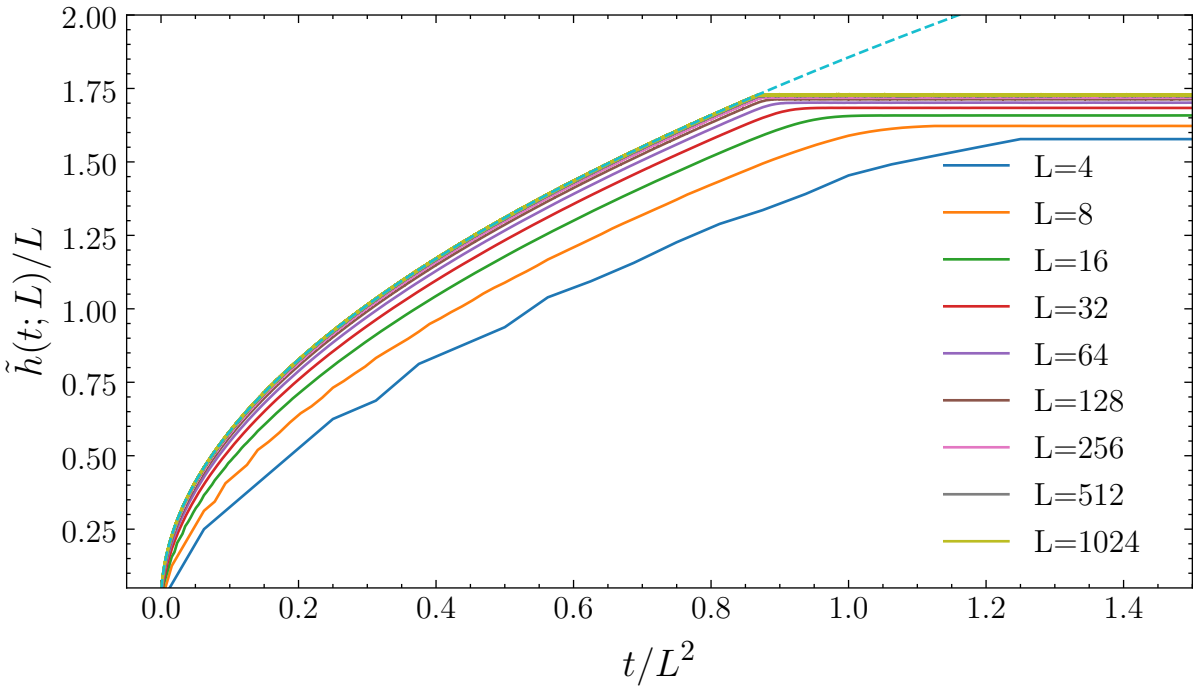

Figure 4: A data collapse for $\tilde{h}$. By plotting $y = \tilde{h}(t;L)/L$ and $x = t/L^2$, this traces out the shape of $\mathcal{F}(x)$. The blue dashed line indicates the best fit for the scaling of $\tilde{h} \sim t^{0.503}$

for some $\alpha > 0$. This must be the case, because $x \gg 1$ corresponds to $t \gg t_c \propto L^2$. Past $t_c(L)$, the system is in the steady state. Thus $\tilde{h}$ stabilises and cannot increase further. For $x \ll 1$, or $t \ll t_c$, $\tilde{h}$ is still increasing. We can imagine the model as a pile filling out a rough, right-angled triangle of height $\tilde{h} < L$ and base $L' \in [\tilde{h}/2, \tilde{h}]$, with one of the vertices fixed at $i = 1$. L' is the highest index i which is filled. Thus, the number of grains t is the area of this triangle, given by

$$t(\tilde{h}) \approx \frac{1}{2}\tilde{h}L'. \tag{6}$$

This approximation improves for $L \gg 1$, such that $z_i \to \langle z \rangle_i$, so that the slope of the pile is smoother. Since L' also contains a factor of $\tilde{h}$, then $t(\tilde{h}) \sim \tilde{h}^2$ and hence $\tilde{h} \sim \sqrt{t}$. This implies $\alpha = 0.5$.

A power-law fit was performed over the transient region, estimated where $t/L^2 \in [0.01, 0.866]$, for $L = 1024$ to best approximate $L \to \infty$ behaviour. The lower bound was not set at 0 because this region significantly deviated from the power-law. This gave the estimate $\tilde{h} \sim t^{0.503} \implies \alpha = 0.503$, agreeing with the theoretical prediction.

The data collapse appears worse for small L, where $\langle \tilde{h} \rangle_t / L$ converges to a lower value in the steady state, and t_c/L^2 is larger relative to the larger L systems. The different $\tilde{h}/L$ value can be found using corrections to scaling. Assume $\langle h(t;L) \rangle_t$ can be expressed as an infinite series in L. Thus, $\langle h(t;L) \rangle_t$ can be approximated as its truncated series:

$$\langle h(t;L) \rangle_t = a_0 L \left(1 - a_1 L^{-\omega_1} + a_2 L^{-\omega_2} + \ldots\right) \quad \text{for } \omega_i > 0 \tag{7}$$

$$\approx a_0 L \left(1 - a_1 L^{-\omega_1}\right). \tag{8}$$

If Equation (8) was divided by L, then

$$\frac{\langle h(t;L) \rangle_t}{L} = a_0 \left(1 - a_1 L^{-\omega_1}\right) \tag{9}$$

$$\approx a_0 \quad \text{for } L \gg 1. \tag{10}$$

Since $\langle \tilde{h} \rangle_t / L$ is just $\langle h \rangle_t / L$ but smoothed out, they converge to the same value of a_0 for $L \gg 1$. However, for systems of small L, $a_1 L^{-\omega_1} > 0$, and is a significant contribution, causing them to converge to a lower value. Recognising this, a fit for $\langle \tilde{h} \rangle_t / L$ for $L = 1024$ in the steady state yielded an estimate $\min a_0 = 1.728$. Specifically, this was a lower bound because fitting on any finite L will result in an underestimation.

2.5 Task 2e

From this task onwards, all estimates were run for $T = 10\,000\,000$. Often, this meant that random errors on each data point were negligible and certainly much smaller than small L effects, so they were no longer part of the error propagation.

To find ω_1 and a_0 in Equation (8), two methods were used. Firstly, the RHS of Equation (8) was fitted directly using a non-linear least squares fit with free parameters ω_1, a_0, a_1. Another method was to rearrange Equation (8) to the form

$$\log\left(a_0 - \frac{\langle h(t;L) \rangle_t}{L}\right) = -\omega_1 \log L + \log\left(a_0 a_1\right). \tag{11}$$

Then, the estimated value for a_0, denoted by $\hat{a}_0$, was tweaked such that a straight line was achieved from the log-log plot of L against $a_0 - \langle h(t;L) \rangle_t / L$. This is because for $\hat{a}_0 \neq a_0$ and approximating $a_0 \approx \langle h \rangle_t / L$ as in Equation (10), then the graph will either cross the $\log L$ axis early, or never cross this axis. Once the graph was straight, a linear fit was performed on the log-log plot, and the negative gradient was used to obtain ω_1. Both methods are shown in Figure 5.

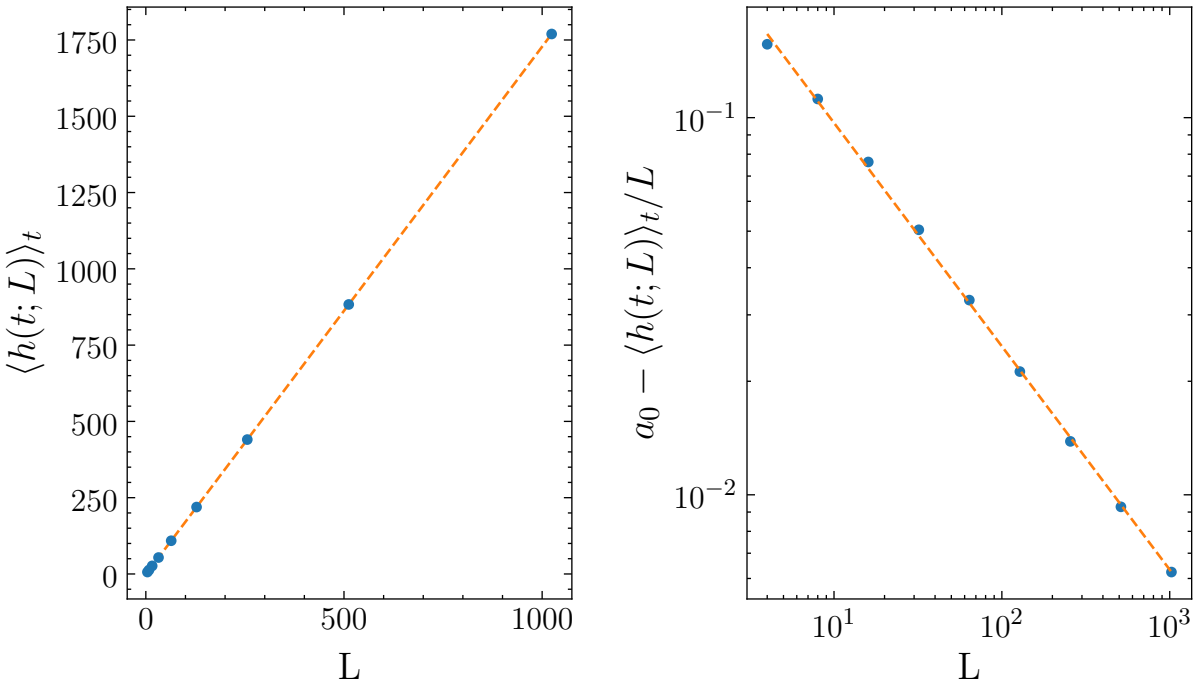

Figure 5: (Left) The orange dashed line is a fit of Equation (8) onto the data. Although it appears linear, corrections to scaling are only noticeable for small L. (Right) shows a second method where Equation (11) was plotted and the estimate $\hat{a}_0$ tweaked to give the straightest line visually. Then a power-law relation was fitted to extract the exponent ω_1.

However, after computing the estimated parameters, both techniques yielded near identical results. This was largely because no value of a_0 could make the data completely straight for the

second method, likely because of the $a_0 \approx \langle h \rangle_t / L$ approximation. Only results from the first method is quoted below for simplicity, and that errors for all parameters were easily obtainable.

$$a_0 = 1.7344 \pm 0.0004$$
$$\omega_1 = 0.596 \pm 0.014$$

The estimate of a_0 here is considerably higher than the $\min a_0$ found in Task 2d, which is as expected. Moreover, these values are only for the truncated series. If more terms in the series were fitted, such as $a_2, \omega_2, \ldots$, the optimal values may deviate to extents not reflected by the quoted errors. However, fitting more terms would introduce too many degrees of freedom for the results to be useful.

2.6 Task 2f

Starting from

$$\frac{h(t;L)}{L} = \frac{1}{L}\sum_{i=1}^{L} z_i(t) \tag{12}$$
$$= \langle z \rangle_i, \tag{13}$$

where the last line is recognised as the mean of z spatially across L sites. Hence, Equation (8) is divided by L to find $\langle z \rangle_i$, and subsequently taking the limit

$$\langle z \rangle_i = \frac{1}{L} a_0 L \left(1 - a_1 L^{-\omega_1} + a_2 L^{-\omega_2} + \ldots\right) \quad \text{for } \omega_i > 0, \tag{14}$$
$$\lim_{L\to\infty} \langle z \rangle_i = a_0. \tag{15}$$

Interestingly, this implies that $\langle z \rangle_i > 1.5$, which may be naively assumed for $p = 0.5$. This is because sites with $z_i^{th} = 1$ topple more often, causing a higher proportion of sites with $z_i^{th} = 1$ to be relaxed compared to $z_i^{th} = 2$. Therefore sites with $z_i^{th} = 1$ have more opportunities to be relaxed and have its slope threshold flipped into $z_i^{th} = 2$ state.

Likewise, assuming the standard deviation for height had a power-law relation, where $\sigma_h = cL^{\gamma}$. This was found to scale sublinearly as shown in Figure 6, with an exponent $\gamma = 0.242$. Furthermore, the relation $\langle z \rangle_i = h/L$ show that h is the random variable $\langle z \rangle$ divided by a constant, L. Therefore, to obtain $\sigma_{\langle z \rangle}$, the same constant is divided,

$$\lim_{L\to\infty} \sigma_{\langle z \rangle} = \frac{\sigma_h}{L} = \frac{L^{0.242}}{L} = L^{-0.758} = 0. \tag{16}$$

2.7 Task 2g

2.7.1 Central Limit Theorem

Assume that in the sample $\{z_1, z_2, ..., z_L\}$, z_i is an identically, independently distributed (iid) random variable with $\mathrm{Var}(z_i) = \sigma_z^2 < \infty$. Then one variant of the Central Limit Theorem (CLT) states that the sample sum $h = \sum_{i=1}^{L} z_i$ is approximately normal $N(L\langle z \rangle_i, L\sigma_z^2)$ for $L \gg 1$ [1]. Therefore, the probability density function of h for a given L, $P(h;L)$, is a Gaussian:

$$P(h;L) = \frac{1}{\sigma_h \sqrt{2\pi}} \exp\left[-\frac{(h - \langle h \rangle)^2}{2\sigma_h^2}\right] \quad \text{for } L \gg 1. \tag{17}$$

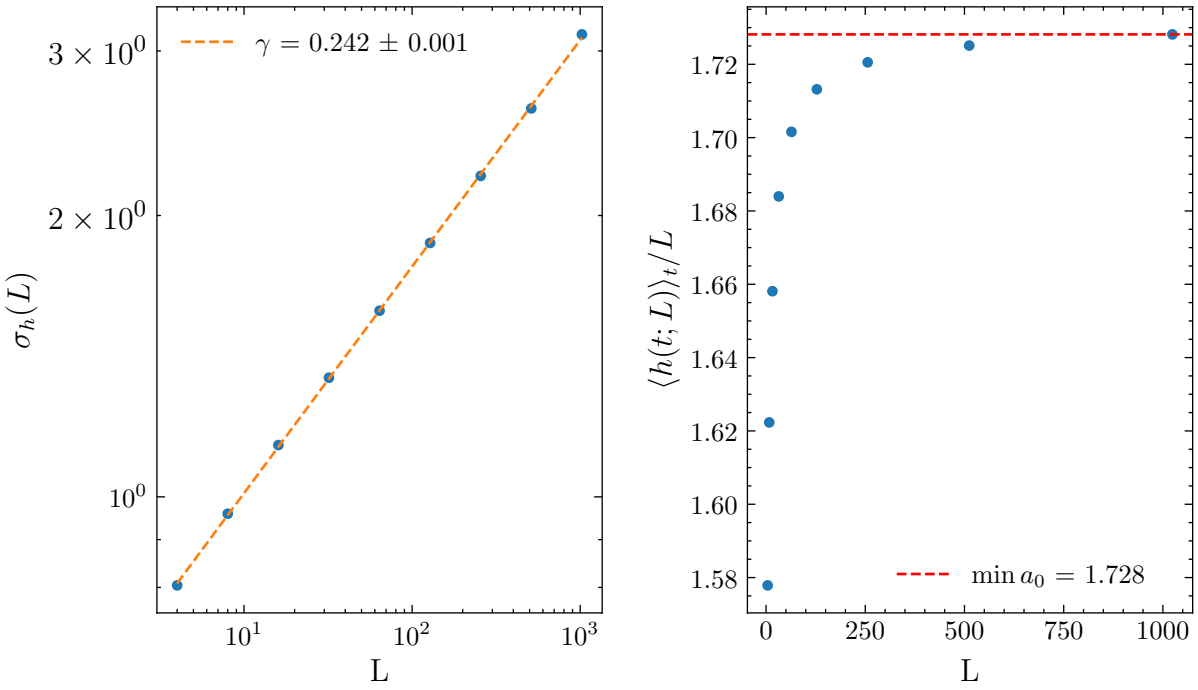

Figure 6: (Left) shows the scaling of σ_h against L after assuming a power law relation to give an exponent. (Right) is $\langle h(t;L)\rangle_t/L$ against L. By fitting a horizontal line on $L = 1024$ to best approximate $L \to \infty$, a_0 can also be found in this graph. However the data points are not in a power law as they did not form a straight line in a log-log plot, and are clearly still increasing for $L = 1024$. Hence this method yields a lower bound with the same reasoning as Task 2d, and gave an identical estimate of $\min a_0 = 1.728$.

The relations $\sigma_h^2 = L\sigma_z^2$, $\langle h\rangle = L\langle z\rangle_i$ can be inferred from the CLT alone. After rearranging, the scaling for σ_h is

$$\sigma_h = \sqrt{L}\sigma_z \tag{18}$$
$$\sim L^{0.5}, \tag{19}$$

where the last line can be made since each σ_z is identical, finite, and constant with respect to L. This does not contradict Equation (16), because $\sigma_{\langle z\rangle_i} = \sigma_z/\sqrt{L}$, the formula for the standard error.

2.7.2 Plotting $P(h;L)$ against h and performing a data collapse

The height probability $P(h;L)$ was plotted against h in Figure 7. A data collapse can be achieved, remembering that the central idea is to transform a function of multiple variables into just one for a scaling function. Firstly, Equation (17) was transformed by

$$\sigma_h P(h;L) = \frac{1}{\sqrt{2\pi}} \exp\left[-\frac{(h-\langle h\rangle)^2}{2\sigma_h^2}\right]. \tag{20}$$

Then this is standardised by setting $x = (h - \langle h\rangle)/\sigma_h$, so that

$$\sigma_h P(x;L) = \frac{1}{\sqrt{2\pi}} \exp\left(-\frac{x}{2}\right) = \mathcal{H}(x), \tag{21}$$

where it is now just a Gaussian function of x, or also known as a standard normal distribution, which will be denoted as a scaling function $\mathcal{H}(x)$. The data collapse is shown in Figure 8.

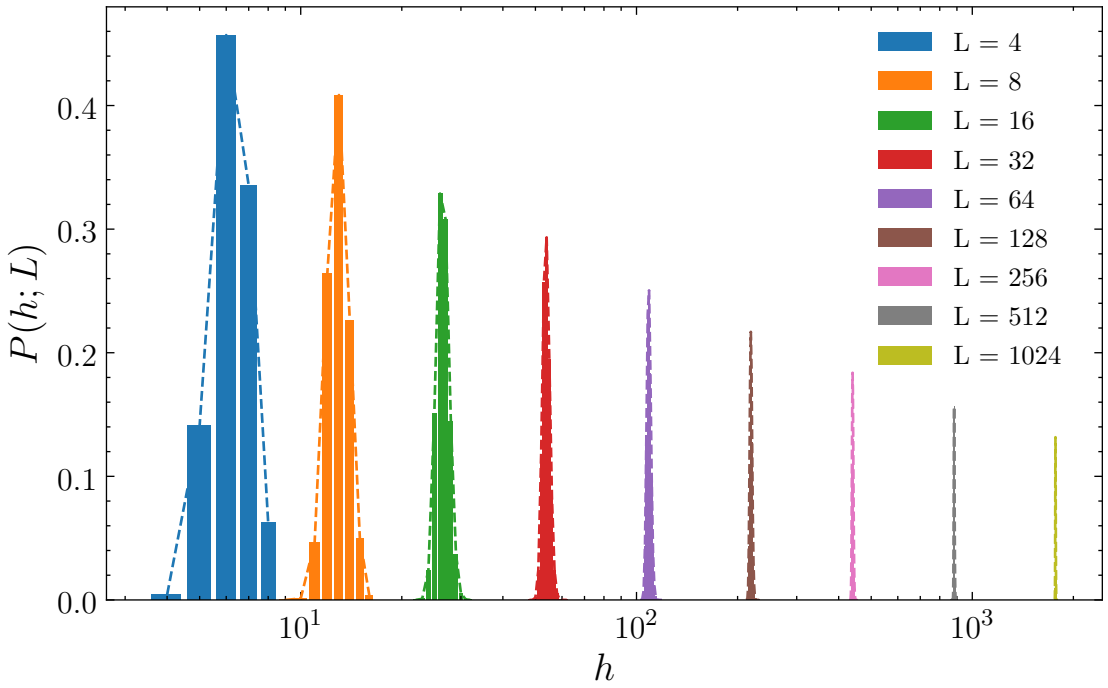

Figure 7: Plot of $P(h;L)$ against h for various L. A dashed outline connects the centres of each bin to improve visibility of histogram outline for high h values.

2.7.3 Evidence that the data does not follow the scaling function $\mathcal{H}(x)$

The data points were expected to follow $\mathcal{H}(x)$. However, a positive skew can be seen from Figure 8, whereas the skew of any normal distribution should be 0. Additionally, Equation 19 does not agree with σ_h found numerically in Task 2f. This implies that z_i is not iid. Specifically, z_i cannot be totally independent, because grains topple from site i to site $i+1$, the next site in the model, suggesting that there must exist some degree of correlation between neighbouring sites. The Kolmogorov–Smirnov test was used as a test statistic, where the null hypothesis tests that the sample is normally distributed [2]. To obtain the sample, $P(h;L)$ was multiplied with T to recover the frequency counts of each $(h-\langle h\rangle)/\sigma_h$ value. The test produced a p-value of 0, which was inferred to be a very small value that caused an underflow in the float. Setting a significance level of 0.05, well above the p-value, the null hypothesis can be rejected.

3 Avalanche-size probability $P(s;L)$

3.1 Task 3a

3.1.1 $\tilde{P}_N(s;L)$ against L

The numerical avalanche-size probability is given by $\tilde{P}_N(s;L)$, where $\lim_{N\to\infty} P_N(s;L) = P(s;L)$, the latter being the true avalanche-size probability. This was measured over N avalanches. However, log-binning was required as N was not large enough to reveal the cut-off t_c, especially for large L where we recall $\langle t_c\rangle \sim L^2$, requiring an exponentially larger t to see the cut-off with increasing L.

Figure 9 shows the log-binned plot. A scale $a = 1.3$ was chosen by eye to best present the result visually, where a controls the rate of exponential increase in length for each bin. Indexing each bin by j, the j'th bin covers the interval $[a^j, a^{j+1}[$. By increasing a, bins cover an increasingly larger interval for larger s, 'catching' the more infrequently measured larger

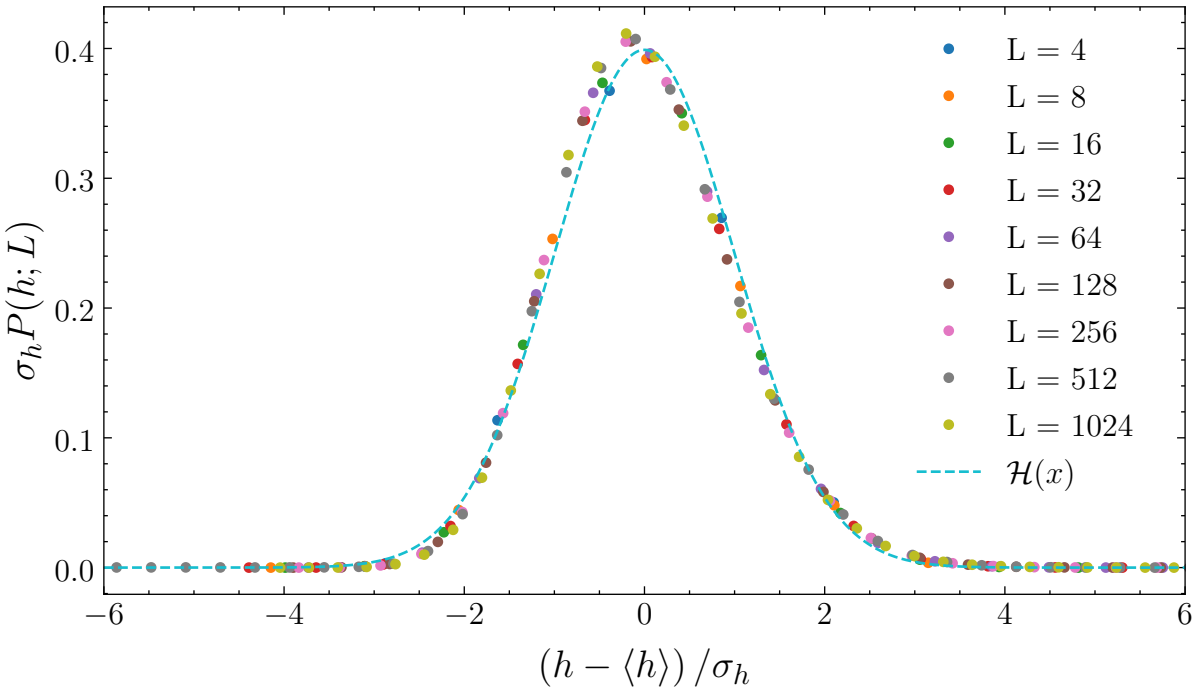

Figure 8: Data collapse for $P(h;L)$ using the measured σ_h and $\langle h \rangle_t$ values. Assuming the Central Limit Theorem, these data points should theoretically follow a standard normal distribution, $\mathcal{H}(x)$, shown in the blue dashed curve. The Kolmogorov–Smirnov test demonstrates data points did not follow a normal distribution, because h and hence z were not independent.

avalanches and thus compensates for the diminishing statistics. Visually this decreases the scatter of points around the power-law relation. However, data points become sparser as the number of bins decrease. The x coordinate of each data point on the plot is the geometric mean of the bin interval, so that the points are equidistant horizontally on the log-log plot.

This plot shows that all models follow the same exponent τ_s when decaying in a power-law relation, as the straight lines overlap. Unlike the data collapses encountered previously, there is a characteristic bump seen when encountering a cut-off s_c, before rapidly falling to 0.

3.1.2 Data collapse for $\tilde{P}_N(s;L)$

A scaling ansatz was proposed to be

$$\tilde{P}_N(s;L) \propto s^{-\tau_s} \mathcal{G}\left(s/L^D\right) \quad \text{for } L \gg 1, s \gg 1, \tag{22}$$

such that $\mathcal{G}\left(s/L^D\right)$ decays rapidly for $s > s_c = L^D$. Hence, plotting $s^{\tau_s}\tilde{P}_N(s;L)$ against sL^{-D} gives the shape of $\mathcal{G}$, shown in Figure 10. To estimate τ_s, $s^{-\tau_s}$ was fitted on Figure 9 for $L = 1024$, in the region $s \in [10, 10^5]$. This region was chosen by eye where the graph appeared straightest. The parameter D was found by visual inspection alone to produce the best collapse horizontally. This gave the values

$$D = 2.20$$
$$\tau_s = 1.543$$

and errors are not quoted as these are estimates only.

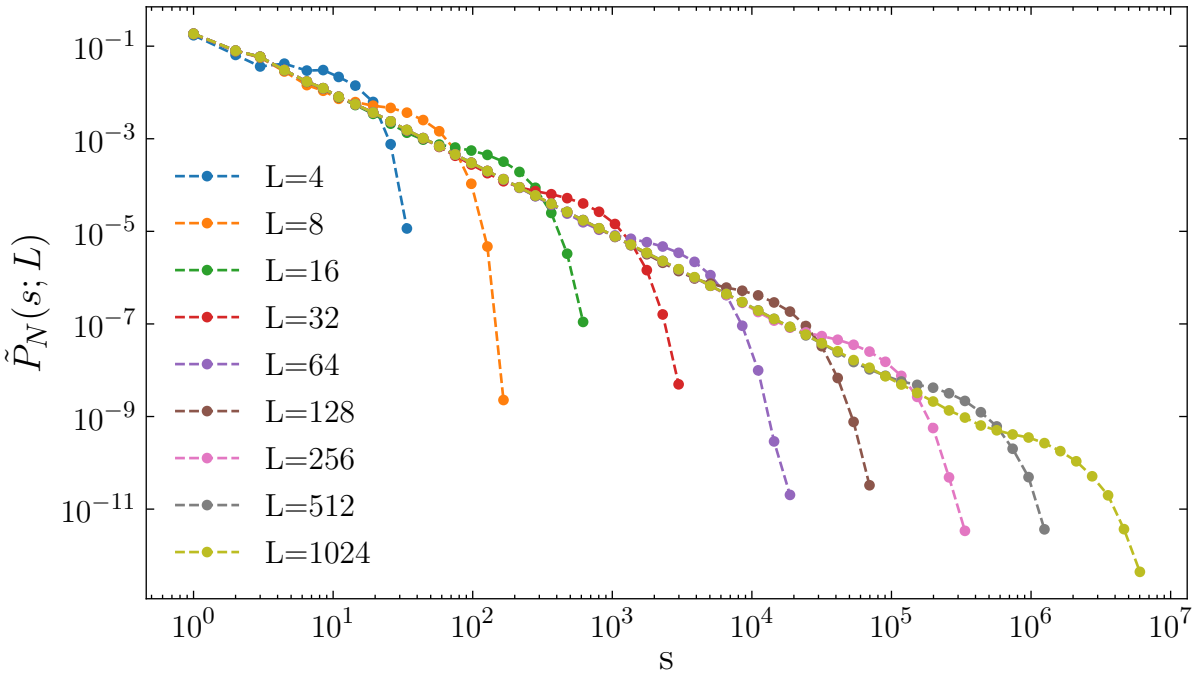

Figure 9: Plot of log-binned probability $\tilde{P}_N(s;L)$ against the avalanche size s, using a log-bin scale of $a = 1.3$, and time ran after the steady state of $T = 10\,000\,000$. For greater L, the straight line extends further before reaching a cut-off avalanche size s_c, implying that the power law relation is valid for a greater range of s.

3.1.3 Task 3b

The average k'th moment over time, s^k, where $k \in [1, 10]$, was plotted in Figure 11. Assuming Equation (22), lectures showed that moments scaled as

$$\left\langle s^k \right\rangle \propto L^{D(1+k-\tau_s)} \quad \text{for } L \gg 1, k \geq 1. \tag{23}$$

Taking logarithms on both sides,

$$\log \left\langle s^k \right\rangle = D\,(1 + k - \tau_s) \log L + \log(\text{const}) \quad \text{for } L \gg 1, k \geq 1. \tag{24}$$

Hence the gradient of each line in Figure 11 give an estimation for $D(1 + k - \tau_s)$ and its associated error. This was only fitted for $L \geq 128$ to reduce small L effects.

A linear fit was performed across these data points, weighted by the reciprocal of the error. From the $k = 10$ moments, this gave 10 data points to fit a straight line upon and is shown in Figure 12. This is equivalent to

$$f(k) = Dk + D(1 - \tau_s). \tag{25}$$

Therefore, the gradient estimate gives D. To obtain τ_s, write

$$\begin{aligned} 0 &= Dk' + D(1 - \tau_s) \\ 0 &= k' + (1 - \tau_s) \\ \implies \tau_s &= 1 + k', \end{aligned}$$

where k' is the k-intercept, $f(k') = 0$. Finally, this produced the results

$$\begin{aligned} D &= 2.2524 \pm 0.0014 \\ \tau_s &= 1.5561 \pm 0.0007, \end{aligned}$$

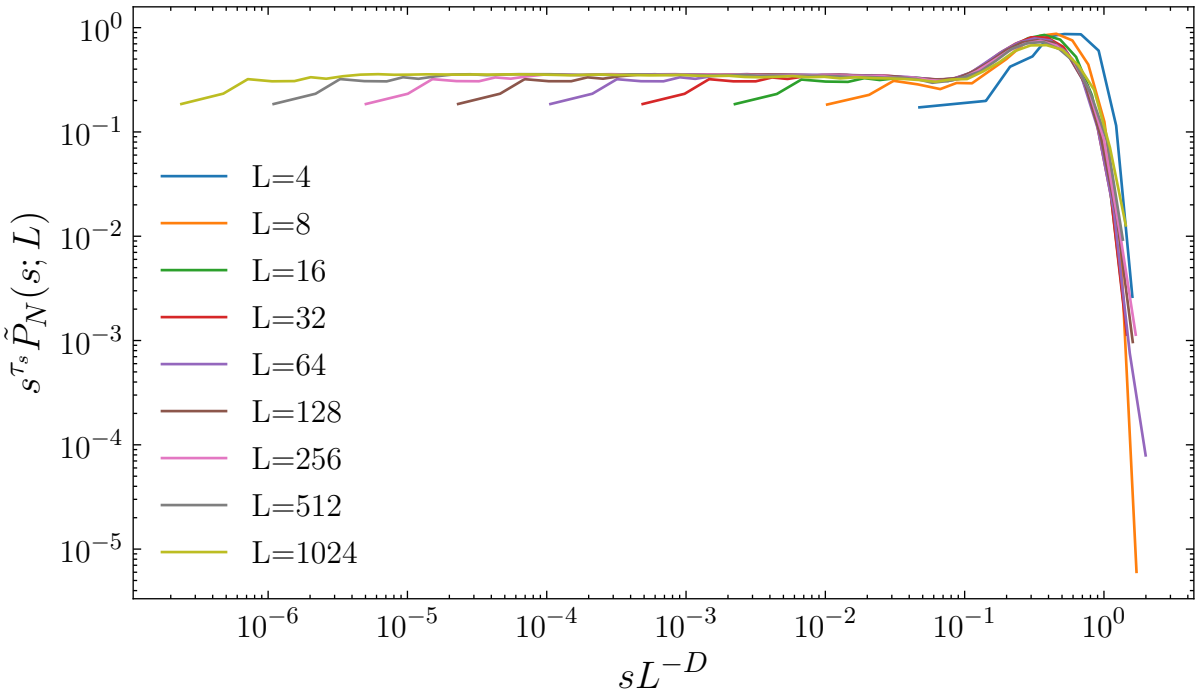

Figure 10: A data collapse for $\tilde{P}_N(s;L)$, tracing out the scaling function $\mathcal{G}$. The parameters were $D = 2.20, \tau_s = 1.543$. Almost all bumps matched, except the blue curve visibly deviated from the rest due to small L effects.

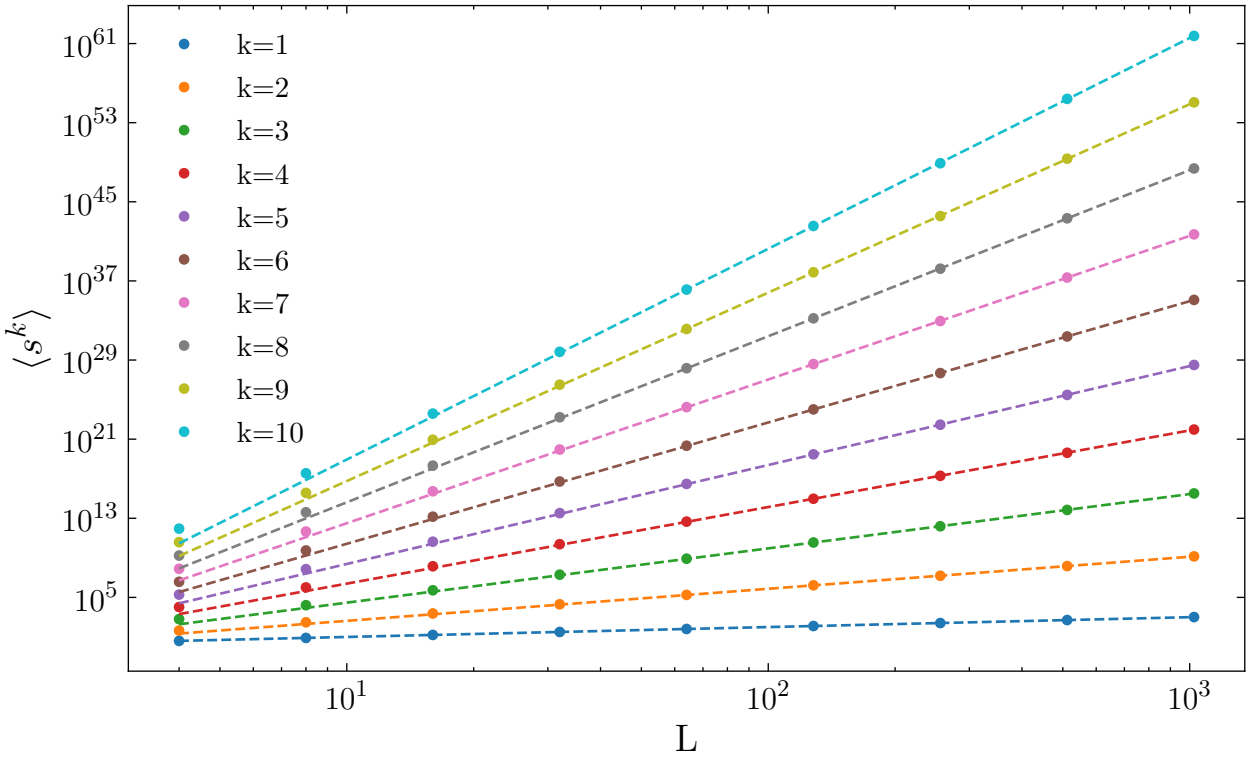

Figure 11: Up to k=10 moments were plotted for different L. Each line connecting the data points was a straight line fit on the log-log plot. All moments conform well as a power law, except that data points towards the left, representing small L, are all seen to lie above the lines, indicating small L effects are significant.

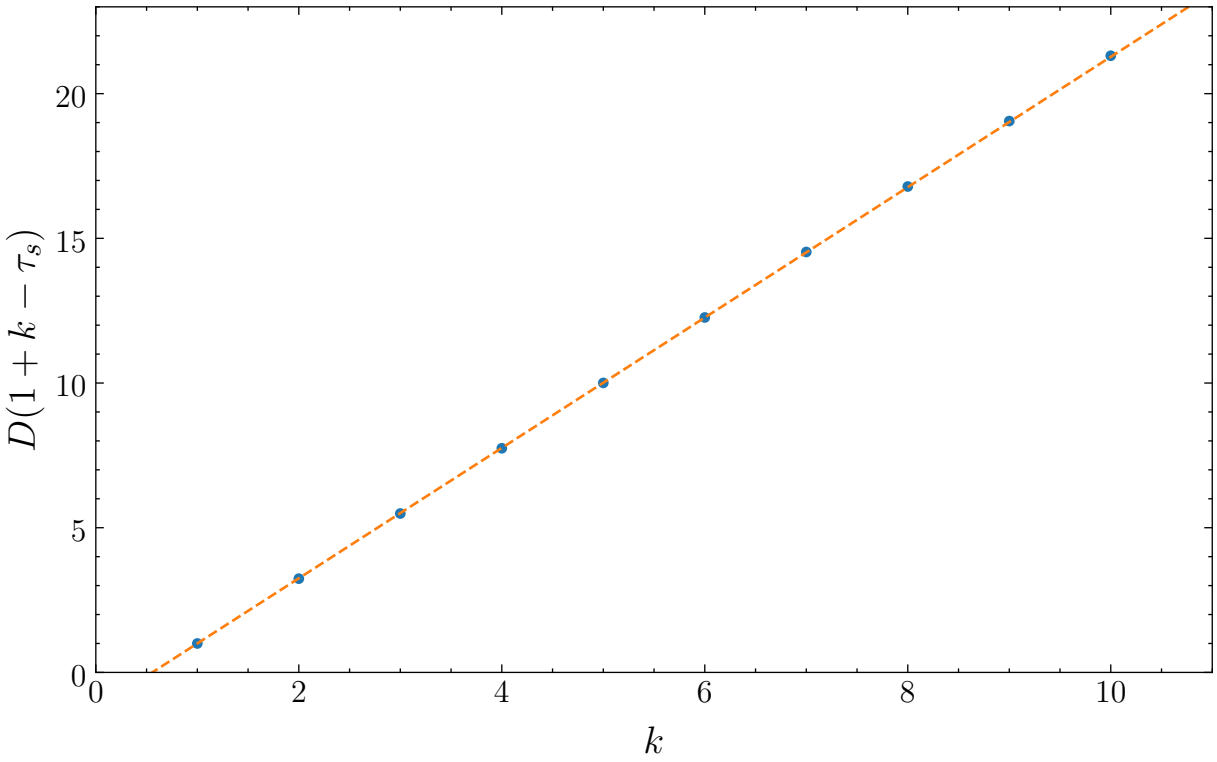

Figure 12: Each k from Figure 11 become a data point in this plot. The gradient and k-intercept give estimates for $D = 2.2524 \pm 0.0014$ and $\tau_s = 1.5561 \pm 0.0007$ respectively.

which matches closely with values found in Task 3a, values in lecture notes of $D = 2.252$, $\tau_s = 1.557$, and conjectured values of $D = 9/4$, $\tau_s = 14/9$ in literature. Just as in lectures notes, our values fulfill the condition D(2-τ_s) = 1. These exponents and the data collapse together demonstrate the scale-free nature (with respect to L) of the Oslo model. The multiple exponents arising from simple local relaxation rules on z also exemplifies self organised criticality.

4 Conclusion

From the investigation, several scaling relations were theoretically predicted, and cross-checked with the numerically simulated model. The avalanche size exponents were also verified with literature, giving confidence that results were correctly computed. Further improvements could be made by simulating larger L to better approximate $L \gg 1$, or alternatively find a bound for the error that arise due to finite L effects to be included in the error propagation. Additionally, after concluding z_i is not independent, it is worth investigating the exact dependence of each z_i with the other slopes, such as by plotting an autocorrelation function.

References

[1] W. Monroe. "Central limit theorem." (Aug. 2017), [Online]. Available: https://web.stanford.edu/class/archive/cs/cs109/cs109.1178/lectureHandouts/190-central-limit-theorem.pdf (visited on 02/18/2023).

[2] "Scipy.stats.kstest — SciPy v1.10.0 manual." (), [Online]. Available: https://docs.scipy.org/doc/scipy/reference/generated/scipy.stats.kstest.html (visited on 02/19/2023).